FRP strengthening of web panels of steel plate girders against shear buckling Part-I: Static series of tests

FRP Strengthening of Web Panels of Steel Plate Girders against Shear Buckling Part-I: Static Series of Tests

Zaid Al-Azzawi[1], Tim Stratford[2], Michael Rotter[2], Luke Bisby[2]

[1] College of Engineering, The University of Anbar
P.O. Box 55/ Ramadi (55431/Baghdad)- Anbar- IRAQ.

[2] School of Engineering, The University of Edinburgh.
AGB Building, The King's Buildings, Mayfield Road, Edinburgh, EH9 3JL, UK.

Corresponding author: Zaid Al-Azzawi
Email: zaidkani@yahoo.com – zaid.kani@uoanbar.edu.iq

ABSTRACT

The result of an experimental programme investigating a novel technique to strengthen web plates against breathing fatigue is presented in this paper; the programme was divided into five phases, including: (1) the development of a novel preformed corrugated FRP panel for strengthening thin-walled steel plate girder webs against buckling, (2) selecting the adequate adhesive and epoxy using double-lap shear and tension specimens, (3) producing the FRP panel, and (4, 5) testing its performance in two main experimental series; the initial (static) series and the final (cyclic) series. Only the initial series which involved tests on 13 steel plates strengthened with the proposed preformed corrugated FRP panel and subjected to in-plane shear will be reported in this paper. This series investigated the performance of different forms of strengthening under static load, in preparation for a subsequent series of cyclic tests to investigate their fatigue performance. Test results showed the efficiency of the technique at increasing the stiffness of the strengthened specimens in comparison to the unstrengthened ones and reducing the critical stresses which will serve as a precursor for the anticipated increase in the fatigue life of the girders.

KEYWORDS:

Plate girders; Steel plates; FRP; Buckling; Shear.

INTRODUCTION

Strengthening of structures has received increased attention within the construction community in recent decades. Structural strengthening may be required due to:

- change of specifications including re-zoning of seismic risk and wind distribution, or changes in design philosophy;
- load increases, especially for bridges and industrial buildings;
- design or construction errors; and
- damage to structural elements caused by deterioration of construction materials or the application of unexpected loads such as fire, earthquake, or impact (Assoodani, 2014).

Steel and composite steel-concrete bridges constitute a large number of the existing bridges worldwide. In 2008, it was reported that about 12% of total number of bridges (72,520 bridges) in the United States were structurally deficient (Bureau of Transportation Statistics, USA, 2008). Steel bridges comprise about 50% of the structurally deficient bridges. The need for adopting durable materials and cost-effective strengthening techniques is therefore self-evident.

Different techniques exist for strengthening structures; all of which have drawbacks. For instance, conventional techniques for strengthening steel structures – like welding additional transverse/longitudinal stiffeners – require heavy equipment during installation, their fatigue performance can be of concern, and may be a need for ongoing maintenance due to corrosion attack. Amongst the available strengthening techniques, the use of fibre reinforced polymers (FRPs) is appealing because of their resistance to corrosion, low weight, and high tensile strength.

The use of these composite materials for structural strengthening of both steel and concrete structures is seen as a promising technology. However, most of the work to date has been focused on concrete structures. The key reason for the less common use of FRPs for strengthening steel structures is their comparatively low tensile modulus of elasticity. This means that either a more costly high modulus carbon fibre reinforced polymer (CFRP), and/or a greater thickness of FRP material is needed for strengthening. By adding externally bonded FRPs, the stress levels in the original member may decrease, thus resulting in a longer fatigue life.

Typically, flexural strengthening with FRP is straightforward as the FRP is bonded along the tensile flange to take full advantage of the strengthening FRP material. However, shear

strengthening is not similarly straightforward because of the multi-axial stress state under shear condition. Most of the shear stress is resisted by the web on the basis of tension-compression diagonals and a smart technique needs to be implemented to take best advantage of the FRP material because it does not perform well in compression in comparison to its superior tensile properties, never mentioning the web buckling problem which might lead to early deboning if not considered in the design.

The project presented in the current paper examines strengthening of the webs of steel plate girders against shear buckling using externally bonded FRPs. In-plane loading of thin web plates close to the shear buckling load results in out-of-plane displacements, which in turn induces secondary bending stresses at the welded web plate boundaries. Under repeated loading the combined state of membrane and secondary bending stresses may result in fatigue cracking and failure. In the current work, an FRP strengthening technique using bonded shapes is applied to resist these out of plane deformations by stiffening the steel plate, rather than to provide additional direct tensile strength (as is the case in flexural strengthening), Fig. (1).

BACKGROUND

Roberts et al. (1995a) noticed that during fatigue tests the girders exhibited considerable web plate breathing, with pronounced shear buckles forming and reforming along the tension diagonals of the web panels during cyclic loading. Fatigue cracks formed along the toes of the welds between the web and boundary members, in regions of high secondary bending stresses caused by out-of-plane (buckling) deformations. The number of load cycles to fatigue crack initiation varied considerably; for higher load ranges the rate of propagation of fatigue cracks was reasonably uniform, while for lower load ranges it was variable.

On the basis of their research, Roberts et al. (1995b) stated that stress ranges at potential fatigue crack locations could be predicted using nonlinear finite element analysis (FEA) or approximate analytical solutions. They also showed that the fatigue assessment procedures recommended in the Eurocodes, based on either principal stress ranges or normal and shear stress ranges, provided conservative estimates of the fatigue life for slender webs subjected to plate breathing.

Skaloud and Zornerova (2005) continued to study fatigue of slender plates. They studied the limit state for the webs of steel plate girders subjected to repeated loading, and stated that the response is affected by the cumulative damage process generated in the web under repeated loading.

Patnaik and Bauer (2004) studied the effect of shear and flexural strengthening in steel beams using CFRP covering. Thirty–percent increase in load bearing capacity was observed in beams which went under tests for flexural strengthening using CFRP on tensile flange while 62-percent increase in shear capacity was observed for beams used for studying the shear of CFRP strips in the beam web.

Limited numbers of researchers have studied strengthening of steel plate girders under short term shear loading. One such study is by Okeil et. al. (2009), who investigated the use of externally bonded GFRP pultruded sections for strengthening steel structures. The GFRP sections were bonded to thin-walled steel plates in orientations that contributed to the out-of-plane stiffness of the plate rather than its in-plane strength, as is the more common practice in FRP strengthening applications. Beam (shear) specimens were tested to explore the out-of-plane strengthening technique, increasing the ultimate capacity of the strengthened specimens by 56%; however reducing their ductility.

Miyashita et al. (2012), also conducted a series of shear buckling tests on seven steel plate girders with CFRP sheets bonded to both sides of the web panel as a substitute for material lost due to corrosion attack. Test variables included the web aspect ratio (a_w/d =1 and 1.5) and the plate slenderness ratio (h_w/t_w = 133 and 166). Different numbers of fabric layers and fibre angle orientations were used. An increase in the ultimate capacity of the specimens, between 6.18 and 29.19 percent, was reported, along with a proposed modification to Basler's equation (Basler, 1961) to account for the addition of bonded CFRP showing a good correlation with test results.

Bhutto (2013) presents similar testing on eight CFRP and GFRP strengthened plate girders. The CFRP used was carbon fabric sheets applied in layers by a wet layup process, while the GFRPs used were T and I-sections adhered vertically and diagonally to the web plate to act as substitutes for steel stiffeners. The ultimate loads were increased by 1.20 to 1.54 times due to FRP strengthening.

OPTIMIZATION OF THE STRENGTHENING TECHNIQUE

Analytical Model

Fig. (2) provides details of the analytical model adopted in the current study. The initial plate shown in Fig. (2-a) is a square steel plate of 500×500mm having a slenderness ratio (h_w/t_w) of 250, where h_w and t_w represent the height and thickness of the steel plate, respectively. Figs. (2-b) and (2-c) show the classical (i.e. flat sheet) and proposed (i.e. profiled) FRP

strengthening techniques, respectively. In the classical technique, several layers (plies) of FRP are bonded using wet-layup process usually over the entire area of the steel plate, to produce a composite section with greater stiffness. The strengthening technique used here is based on a preformed corrugated FRP panel bonded to the compression diagonal of the web plate, which is a more efficient use of FRP material due to the higher flexural rigidity of the profiled shape. Preliminary FEA confirmed that the specimens strengthened with the proposed diagonal corrugated profiled FRP panel had higher stiffness and critical buckling shear stress.

Cross-Section of FRP Profiled Plate

Figs. (3-a and b) show three selected types of corrugated profiled FRP plates; with rectangular, semi-circular, and half-hexagonal profiles, respectively. Several preliminary trials have been made before these ones using hand calculation techniques to optimize the corrugation section with different shapes, heights, widths, and number of corrugations per section. These calculations were based on Euler strut model in axial compression and plates under pure shear conditions. The sectional dimensions of the panel were chosen to consume the least possible FRP material and bonding epoxy quantities, whilst not providing excessive geometrical stiffness, which might lead to brittle failure like most other FRP strengthening techniques. The chosen preformed corrugated FRP panels had typical widths of 195mm, with variable lengths and end cut shapes. Perfect bond was assumed between the FRP and the steel plate in all modelling cases for optimizing the corrugation geometry.

Each of the three profiled shapes was tested numerically using elastic bucking analysis available in the FEA code *Abaqus*. The FRP panels were assumed to be made of GFRP laminate with a thickness of 1.4mm and a modulus of elasticity of 14.4GPa. The FRP section was bonded (tie constrained) to an S275 steel plate having dimensions of 615×245×2mm. Fixed boundary conditions were imposed at both ends of the steel plate, except for the in-plane axial displacement at the loaded edge. This plate was used to represent a compression diagonal strip from the steel plate as shown in Fig. (3-c). A reduced integration linear 4-noded shell element (S4R) was used for both the steel and the FRP.

The results of this preliminary FEA showed that Euler critical buckling loads were 10.3kN, 7.3kN, and 8.4kN for the steel plates strengthened with the rectangular, semi-circular, and half-hexagonal corrugated sections, respectively. In spite of the fact that the rectangular section had the highest buckling load, it was excluded from the results because it is thought that the sharp edges of this section will act like stress concentrators for both FRP composite

and the bonding strips. The semi-circular and half-hexagonal profiled sections were chosen for further numerical investigation.

At this stage it is worthwhile emphasizing that choosing the right geometrical properties for the FRP strengthening panel is not an easy and straightforward process. Different variables need to be taken into considerations for a successful optimization criterion including, but not limited to, type of the FRP used, bonding requirement, size of the specimen, required stiffening level, and some practical considerations with respect to applicability in the field. Based on the observations in this study, it is recommended to limit the second moment of area of the stiffening FRP section so that the ultimate shear capacity of the strengthened composite steel-FRP section does not exceed the shear yield capacity of a similar perfectly flat steel plate (the shear yield capacity can be found by multiplying Mises shear stress ($\sqrt{}$fy/3) by the height (h_w) and thickness (t_w) of the steel plate).

Convergence Study

Buckling of thin plates is sensitive to the type of element used in an FEA model. Hence, a convergence/sensitivity study was performed. The model adopted in the convergence study was chosen as a typical web plate with practical dimensions of 2000×2000mm. The variables included the type of the element (S4R, S8R, and S9R5) and the slenderness ratio (h_w/t_w) which was taken as 1000, 500, 250, 200, 166.667, 142.857 or 125, corresponding to plate thicknesses of 2, 4, 8, 10, 12, 14, and 16mm, respectively. Both simply-supported and clamped boundary conditions were investigated, and the shear stress was applied to the plate boundaries exactly as in the main model shown in Fig (2-a).

Fig. (4) shows typical curves for the critical buckling shear stress versus the inverse of the degrees of freedom (dof), for specimens with simply supported and clamped boundary conditions and a plate slenderness ratio equal 250. The dof was calculated according to the number of elements used, and the corresponding dof of each node in the element according to compatibility. Using the inverse of dof provides a prediction of the element size that will give the same theoretical value or as close as possible. S9R5 (which have 5 degrees of freedom at each node: three translations and two in-plane rotations, i.e., no rotations about the shell normal) showed superior behaviour with fewer elements, and a size of $h_w/20$ was chosen; this was sufficiently coarse for economy of the model whilst sufficiently accurate (i.e. close to the theoretical value).

Finite Element Analysis

Fig. (5) shows the predicted buckling modes of the FEA model for a (500 × 500 × 2mm) steel plate strengthened with flat wet-layup GFRP covering the full surface area of the plate, along with buckling modes for the same plate strengthened with either the proposed semi-circular or half-hexagonal corrugated GFRP panels; both having the same thickness and material properties. The critical buckling shear stresses (τ_{cr}) were 43.5MPa, 114.0MPa, and 122.6MPa, for the flat, semi-circular, and half-hexagonal sections, respectively, in comparison to τ_{cr} = 42.5MPa for the initial steel plate with clamped boundary conditions without strengthening.

From the above results, it appears that the new proposed half-hexagonal corrugated FRP panel has the highest buckling stress and therefore it was chosen as the corrugated section to be used throughout this study. The hexagonal section increased the buckling strength by a ratio of approximately three to one in comparison to the control one. A fast parametric study showed that for the classical strengthening technique to achieve the same buckling stress as the proposed one, a 5.9mm thickness GFRP laminate would be required, covering the full surface of the plate. The proposed preformed corrugated FRP panel reduced the required FRP by approximately 8 times (volumetrically) and the required bonding epoxy surface area by 7 times. This did not only reduce the cost of the strengthening process, but it also did not affect the bond strength of the specimen and helped in maintaining the ductile failure associated with un-reinforced steel plate girders.

EXPERIMENTAL PROGRAMME

The objective of the experimental programme was to develop a system to increase the stiffness and strength of web plates. The system in the current work was applied to the web of a presumed end panel in a steel bridge, where high shearing forces are typically exerted. While limited previous work has shown that strength increases are possible for steel structures reinforced with FRPs, relatively little stiffness increase has been observed to date. To provide stiffness increases to thin steel web plates while minimizing material costs, a novel preformed corrugated FRP panel has been introduced (Phase-1). Fig. (6) shows the geometry and orientation of the new preformed corrugated FRP panels.

The experimental programme was conducted in 4 further phases. In Phase-2, saturating resins for wet lay-up of dry fibre sheets and bonding epoxy were selected based on the performance of double lap shear (DLS) coupons that were fabricated and tested in tension. The resin

selected for this process was used in Phase-3 to manufacture the direct tensile specimens which is made to determine the material mechanical properties of the FRP composite.

In Phase-4 (initial test series), thirteen steel plates were strengthened by bonding the new preformed corrugated FRP panel along the compression diagonal of the steel plate, and tested for shear buckling. The in-plane shear loading was applied using a specially designed testing rig "Picture-Frame", that is capable of holding the steel plate in position, applying realistic boundary conditions and in-plane shear loading, to simulate the case of a steel plate serving as the web of a steel plate girder.

Finally, in Phase-5, six plate girders were built and strengthened with the optimized FRP panel from the initial tests and tested to study the behaviour of the proposed strengthening technique under cyclic loading. Preliminary fatigue analysis indicated that the proposed strengthening technique is likely to succeed in reducing the secondary bending stresses in the web plate welded boundaries and thus prolong the life expectancy of steel bridges in failure modes related to web plate breathing (Al-Azzawi et. al., 2015). This conclusion in addition to the experimental results of the cyclic series shall be presented in a separate paper.

FRP Material and Geometrical Properties

Four types of woven FRP cloth were used: Carbon fibre 2/2 twill 12k 450g, carbon fibre 2/2 twill 12k 650g, biaxial glass cloth 440g, and biaxial glass cloth 600g. Table 1 gives the manufacturer specified properties of the carbon and glass fibres.

Two types of carbon and glass fibre sheets were used so as to maintain the same fibre volume fraction (FVF) for the 2 and 3 layer preformed corrugated FRP panels. Although the longitudinal properties of a composite are dominated by the fibre properties, important parameters such as its ultimate elongation will depend also on the saturating resin used, especially when biaxial fabric sheets are used; this will lower the fibre volume fraction in the longitudinal dimension causing the tensile strength and modulus to be reduced. Despite the reduced tensile strength and modulus of elasticity, this distribution still preferable in the more complex stress states such as for shear in thin steel plates.

Double Lap Shear Tests

Double lap shear (DLS) tests were performed for the epoxy selection phase. Test specimens consisted of two plates fabricated from Grade s275 steel, with dimensions as shown in Fig. (7). These were joined together with preformed GFRP or CFRP sheet panels. Surface preparation for the steel consisted of sanding with 120 grit emery paper to achieve a uniform

surface that was free from surface contamination and mill scale. Schnerch (2005) suggested that for the preparation of small areas this provides good mechanical keying suitable for adhesive bonding to steel. Immediately prior to application of the resin, the surface was cleaned with acetone. The plates were clamped using a special jig to maintain their alignment during curing.

During bonding a uniform coating of epoxy was applied to one side of the steel plate in the bonded region, and the FRP panel was placed onto the steel plates, with 25.4mm of overlap on each of the steel plates. The sheets were then pressed into the resin on the steel plates. A 1.9mm gap was left between the steel plates to minimize the effect of end-to-end bonding. Once the resin had cured sufficiently, the same procedure was repeated on the reverse side. Specimens were cured for at least seven days prior to testing. Fig. (8-a) shows the DLS test setup.

Three different epoxies were trialled to find the best one for the wet lay-up process and the bonding process. Epoxy resins tested were EL2 resin, Tyfo s saturant, and Sikadur-330. Table (2) summarizes these tests and the average shear strength for each one. Each value in the table is the average of three tests. The EL2 resin was chosen for saturation while Sikadur-330 was chosen as the bonding adhesive.

Tension Tests

Tension tests were performed to determine the properties of the CFRP and GFRP sheets using the chosen epoxy from the DLS tests. Test panels were fabricated by wet lay-up whereby the dry fibre sheets were saturated with resin bonded onto a flat release board. The fabric sheets then were covered with a peel ply and a breather layer cloth to absorb the extra resin and then vacuum bagged using a 1.0 bar vacuum pump. Using the vacuum bagging process allowed consistent control of the thickness of the panels and the highest possible fibre volume fraction (FVF) within the section.

After sufficient curing the panels were cut into coupons 50mm in width using a tile saw. Pre-manufactured tapered GFRP tabs were bonded to each coupon to prevent premature failure in the wedge action grips of the testing machine. All tabs were adhered using EL2 resin. After adhering, the tabs and adhesive were allowed to cure at room temperature for at least 48 hours before testing.

The FVF of the specimens was calculated based on the weights of the dry fibre fabric before saturation. Prior to saturation, each length of fabric was carefully weighed. After the FRP panels had achieved sufficient working strength, the entire panel was again weighed to find

316 the weight of the added epoxy resin. The fibre weight fraction (FWF) was calculated in this
317 manner and the fibre volume fraction could then be determined from:
318
319 $$FVF = \frac{1}{\left\{1 + \frac{\rho_f}{\rho_r}\left(\frac{1}{FWF} - 1\right)\right\}} \quad \text{..... (1)}$$

where:

FVF = Fibre Volume Fraction.

FWF = Fibre Weight Fraction.

ρ_f = Density of fibres.

ρ_r = Density of the epoxy resin.

320
321 The thickness of each coupon was measured at six locations; the width was measured at three
322 locations. Averages of these were used to determine the cross-sectional area of the coupons.
323 All coupons were tested using an electro-mechanical Instron testing frame, under crosshead
324 stroke control at a rate 1.0mm/minute with data recorded at 1.0 Hz. Strains were measured
325 using digital image correlation (DIC). Specimens were painted with a high-contrast pattern
326 and a series of images were captured at 0.2 Hz using a digital camera (Fig. 8-b). A bespoke
327 DIC algorithm (REF) was used to track the movement of pixel patches in the images.
328 Table (3) gives the mechanical properties of the GFRP and CFRP used in this study along
329 with some other practical aspects, where $\boldsymbol{F_f}$ is the ultimate tensile strength**,** $\square_f$ is Poisson's
330 ratio, and $\boldsymbol{E_f}$ is the tensile modulus of elasticity of the FRP section. Each value typically
331 represents the average of three tests.
332
333 **Manufacturing the FRP Preformed Corrugated Panels**
334 As mentioned earlier, In order to provide stiffness increase to the thin steel plates while
335 minimizing the cost of the applied material, a new preformed corrugated FRP panel was
336 introduced.
337 The Hex preformed corrugated sections were made by wet layup process of the two types of
338 CFRP and GFRP fabric sheets for two and three layers in an attempt to maintain the same
339 FVF for all specimens. Vacuum bagging was adopted because of the difficulty of moulding
340 the hexagonal section with traditional techniques, see Fig. 9. It is worth mentioning that both
341 open and closed sections were made from GFRP and CFRP as shown in Fig. (6-b), however,
342 the closed section were made with two FRP layers only. This was done to see if the open
343 section would cause any lack of bonding due to its lesser adhesion area.

Development of the Test Method

The classical method to test the shear panel of a plate girder is by testing small or large scale plate girders, combining the two end panels into one plate girder because the end panels represent the most critical shear loading along a plate girder's span; see Fig. (1). However, this is considered a very costly method because each time a variable is changed a new specimen has to be tested.

In the current work a new testing rig (Picture-Frame) is introduced. This picture-frame is capable of holding the steel plate, applying fixed boundary conditions and in-plane shear loading, simulating the web of a steel plate girder; see Fig. (10). It is based on the idea of clamping the steel plate boundaries into a stiff steel frame using bolts that do not pass through the steel plate itself to avoid stress concentrations. It is capable of moving only in-plane using a 4-hinged beam-chain mechanism and thus applies shear force on the steel plate relying only on friction between the picture-frame and the steel plate. The in-plane movement is achieved using 8 mirrored hinges (instead of 4) to avoid cutting the steel plate corners which will affect the stress distribution and to make sure that the loads are applied throughout the plate corners for better simulation of buckling of steel plates under pure shear loading.

The validity of the design for the picture-frame rig was established using finite element simulations that included modelling different scenarios with respect to the boundary conditions applied to the steel plate, the location of the hinges, and the distribution of the stresses developed in each component of the frame and the tested steel plate. Figure (10-b) shows the final finite element model.

Test Variables

The parameters varied in the current study were the type of FRP (CFRP or GFRP), the number of layers of fabric for the same fibre volume fraction, the bonded length along the compression diagonal, the FRP panel section (open vs. closed section), the orientation of the glass fibres, and the shape of the preformed panels' end cut. These are shown in Table (4); along with the ultimate test loads for the specimens tested in the initial static series- refer to Fig. (6) for additional details. Thirteen 500x500x2mm steel plates, having a modulus of elasticity (E_s) of 190GPa and a yield strength (f_y) of 245MPa, were strengthened with the proposed preformed corrugated FRP panels and tested using the picture frame rig. The plates had a constant aspect ratio (a_w/h_w=1.0) and slenderness ratio (h_w/t_w= 250).

Specimen Preparation

Except for the control specimen, which was not strengthened, the following procedure applies for all other specimens (Table 4). First the specimen was grit blasted to the required texture and then cleaned of contamination using acetone. The adhesion energy of the surface was determined using a 20mm dolly with digital adhesion tester. Adhesion tests were performed after 24 hours and 7 days of curing at room temperature, respectively. The adhesion strength varied between an average of 7.65 MPa and 8.21 MPa for the 24 hour and 7 day tests, respectively. The epoxy was then mixed and applied to the steel plate and the FRP panel after removing the peel ply cloth, which helped keeping the FRP panel uncontaminated with a good bonding texture. The FRP panel was attached to the specimen using a special fixture to hold it in position. Finally, a uniformly distributed load was applied to press the panel toward the steel plate to reduce possible air bubbles and maintain a uniform epoxy thickness. The load was maintained for 24 hrs and then removed.

Test Instrumentation

Fig. (11) shows the specimens, testing rigs, and test instrumentation for the initial series of tests. A single strain gauge rosette was used in the centre of the plate to record the vertical, horizontal, and diagonal strains. The strain gauge readings along with the eight displacement gauges (LPs) were recorded at a rate of 1.0 Hz. The location of the LPs and strain gauges are shown in Fig. (11-c) where S refers to strain gauge and LP refers to linear potentiometer.

Five of the 30mm LPs (LP1-LP5) were used to determine the plate out-of-plane displacements, while two 30mm LPs (LP6-LP7) ensured that there was no rigid body rotation for the picture-frame, and one 100mm LP (LP-8) was used to determine the deflection at the bottom end of the plate. Tests were performed using a 1000 kN servo-hydraulic actuator at a stroke rate of 1.0 mm/minute.

EXPERIMENTAL RESULTS

Table 4 shows the test results for the thirteen plates tested in this initial series of tests. From this table, it can be seen that for the strengthened specimens, the ultimate capacity is slightly increased between 5.6% and 24.1% depending on the type of the FRP panel used in strengthening them. The lowest strength increment (5.6%) resulted from strengthening the steel plate with GFRP-2L-(45°-45°)-A (SP-2) while the highest increase in strength is achieved using CFRP-2L-(0°-90°)-C (SP-13). This relatively low increment in the ultimate capacity of the FRP strengthened steel plates might be attributed to the fact that the proposed

412 strengthening technique in the current work is originally designed to increase the stiffness
413 and buckling strength rather than increasing the ultimate capacity of the strengthened
414 specimen as will be discussed in detail later in this section.
415 The ultimate load is defined as the load where the specimen starts to undergo high
416 deformations without the need to increase the applied shear load significantly. In most cases,
417 the loading curve managed to reach a horizontal plateau representing yielding of the steel
418 plate and in some other cases the loading curve reached to something similar to a yielding
419 plateau but with some minor load increment due to strain hardening of the steel plate and the
420 stiffening effect of the FRP panel. In a few cases the test was stopped for technical and safety
421 reasons when the deformations were very high or when the load reached a level that could
422 affect the testing rig. This latter case took place only once with testing SP-13. However, the
423 buckling load is not very straightforward to determine like the ultimate load and needs more
424 investigation.
425 For the control specimen, the buckling load is estimated to be around 40.0 kN using the
426 change in slope method compared to the theoretical 42.5 kN for plates with clamped
427 boundary conditions. However, the buckling load for the strengthened specimens could not
428 be detected because the out-of-plane displacement behaviour was significantly altered and
429 neither the change in slope nor Southwell method is applicable for determining the buckling
430 load. This will be discussed and more investigated in the following section.
431
432 **Central Out-of-Plane Buckling**
433 Fig. (12) shows the load versus out-of-plane displacement for each of the 13 specimens. From
434 this figure, typical patterns of behaviour can be detected. For the control specimen the
435 behaviour is tri-linear where the curve starts linearly at the initial stage of loading then it
436 suddenly changes slope indicating the critical buckling shear stress. After first buckling, the
437 web buckles sideways and only the diagonal in tension is working. This results in the
438 formation of wrinkles, and instead of the pure shear state before buckling occurs; simple
439 tension exists in the wrinkle direction (i.e. diagonal tension). The development of the tension
440 field results in a post-buckling reserve of strength, as illustrated by the non-linear part of the
441 curve for the control specimen in Fig. (12). Since the limit for the steel in tension is its yield
442 strength, the specimen continues to resist shear loading until the diagonal tension yields; this
443 is demonstrated by the upper flat portion of the curve in the figure.
444 The behaviour of the strengthened specimens is different and from Fig. (12), it can be divided
445 into three categories depending on the type of the FRP panel used. The first category

followed the tri-linear behaviour of the control specimen but with a stiffer response, a good example of this type of behaviour is the CFRP strengthened specimens in Fig. (12-a). The second category showed a bilinear response where the linear initial stage of loading continued without showing any sign of buckling until it reached close to the ultimate capacity where it curved dramatically towards the failure plateau. This bilinear type of behaviour can be seen in the GFRP strengthened specimens in Fig. (12-c). Finally, the third category is associated with specimens which altered their predesigned failure mode to a reversed buckling mode in the opposite direction. This reversed buckling mode can be seen in the GFRP strengthened specimens in Figs. (12-c and 12-d).

Generally, due to the proposed unsymmetrical way of strengthening the plate from one face only, there is an induced pre-buckling mode which succeeded (most of the tests) in forcing the buckling mode to the FRP face farthest away from the steel plate where the maximum tension stresses exists, and this increases the efficiency of the strengthening technique because FRP is superior in tension. This helped in reducing the out-of-plane displacement and reduced the secondary bending stresses, especially within working stress.

For the control specimen, the experimental buckling stress was approximately 40.0 MPa. The value of 40.0 MPa is calculated by dividing the buckling load (40 kN) by the plate sectional area. However, this is just an average number estimated from the zone where the bucking curve extremely changes in slope beyond the initial linear stage, and is not based on any engineering calculations. Nevertheless, this buckling load can be detected form the diagonal tension strain curves as well where a sudden change in the curve slope can be seen around this load announcing the development of the tension field.

With respect to the strengthened specimens, no buckling loads could be determined from Fig. (12) due to the significant alteration in the typical behaviour of shear buckling as a consequence of the proposed strengthening technique. This fact will be further supported by the finite element model where no buckling load can be detected as well. In some curves within Fig. (12), there are some indications for the development of the tension field in the tested plates. This is postulated to be caused by a minor slip in one of the tension corners of the picture-frame testing rig in some of the tests.

Typical photos for specimens after failure are given in Fig. (13). These photos were taken after the picture-frame was dis-assembled and the steel plate is taken out. Form these photos, it can be seen that the proposed strengthening technique succeeded in reducing the out-of-plane displacement and changed the buckling mode.

480 ***Effect of the Strengthening Section and FRP Material Type***

481 Fig. (12-a) is a comparison between the open and closed FRP panel sections. It is clear that
482 the closed section FRP panels were not significantly stiffer than the open section ones, even
483 though these had higher second moment of area and much larger bonding area.
484 The initial response is slightly different and it is postulated that it is due to a minor gripping
485 slip in the tension diagonal, mainly with testing specimens SP-2 (GFRP-2L-(45°-45°)-A) and
486 SP-3 (CFRP-2L-(0°-90°)-A). This may have caused a small slack in the specimen, causing the
487 curves to turn concave down during their initial stages until the slack was taken up. The slip
488 took place because there was no mechanical anchorage between the plate and the picture-
489 frame and the grip was solely dependent on the friction according to the original design. For
490 the remaining tests, eight 16mm diameter bolts were added to the picture-frame to ensure that
491 the steel plate was effectively clamped and the slip prevented in the initial stages. However,
492 this precaution caused the load to fluctuate at the final stages for some of the tests (referred to
493 with dashed lines in the figures).
494 Fig. (12-a) also shows that the CFRP and GFRP strengthened specimens had similar stiffness
495 in the initial loading stages, while the CFRP ones had higher stiffness during later loading
496 stages. This is expected because in the initial loading stages the plate is not yet buckled and
497 the stiffness of the strengthening material plays a limited role; however for higher loading
498 stages (after the specimen has already buckled), the stiffness of the strengthening material
499 plays a major role as it reduces the out-of-plane displacement.
500

501 ***Effect of the FRP Number of Layers***

502 Fig. (12-b) illustrates the effect of increasing the number of FRP layers for the same fibre
503 volume fraction. From this figure it can be seen that the three-layer GFRP panels were more
504 effective in the initial stages but had the same stiffness in the later stages. However, the three-
505 layer GFRP panel showed more integrity and did not crack at the ultimate load the way the
506 two-layer GFRP one did; this can be seen by comparing the failed specimens' photos in Fig.
507 (13-a). In contrast, the three-layer CFRP panel behaved almost the same as the two-layer one
508 and had even lower ultimate capacity.
509

510 ***Effect of Glass Fibre Orientation with respect to the Axis of Corrugation***

511 Fig. (12.c) shows the effect of the fibre orientation for the GFRP panels. It can be seen that
512 changing the glass fibre orientation from the default of this work, (i.e. 45˚/45˚) to 0˚/90˚ had
513 no clear effect on the results of the 3-layered GFRP specimen (SP-9) but affected the two-

layered 0˚/90˚ GFRP specimen (SP-8) which had a very stiff but brittle behaviour and led to an alternative mode of failure in the opposite direction to that expected. This could be justified by examining the failed specimen photo in Fig. (13-a) where it can be shown that the FRP panel cracked near the bottom compression corner causing the specimen to alter its buckling mode because this corner usually suffers from severe deformation due to the thrust effect of the sharp triangular end cut associated with type-A FRP panels.

Effect of the End-Cut Shape and Position

Fig. (12-d) shows the effect of the end-cut shape and position for the FRP panels. It can be seen that in the case of GFRP the round cut (Type-B) succeeded in increasing the stiffness of the specimen in both the initial and final stages of loading, in addition to increasing the ultimate load capacity. In the case of CFRP, the round end-cut (Type-B) did not obviously improve the behaviour. The same observation does not hold for the longer FRP panels with triangular end-cuts (Type-C). This type of panel only improved the stiffness of the specimen in the initial loading stages, while the direction of the buckling was reversed in the higher loading stages (i.e. beyond 80 kN). Nevertheless, the CFRP long panel with triangular end-cuts (Type-C) improved both the stiffness and ultimate capacity; however the test was halted when the applied load exceeded 173 kN (for technical/safety reasons).

In-Plane Deflection

Figs. (14-a) to (14-d) show the load-deflection curves in four categories, as was the case for out-of-plane buckling. Fig. (14-a) shows the effect of using closed sections versus open sections, in addition to the bonded area available for bonding the FRP panel to the steel plate. Fig. (14.b) shows the effect of using two-layer FRP panels versus three-layer panels. Fig. (14.c) shows the effect of fibre orientation for GFRP panels, and Fig. (14.d) shows the effect of end cut on the deflection response. From these figures it appears that no obvious trends can be indicated, except that generally the strengthening technique insignificantly increases the stiffness, ductility and ultimate capacity. This leads to the question of whether deflection curves or buckling curves should be used to determine stiffness and energy absorption capacity of the strengthened specimens. By examining the buckling curves and comparing them to the load-deflection curves, it is self-evident that buckling curves are more representative when it comes to shear buckling failure and should be used instead of the usual approach of using the load-deflection curves.

Assessing the Stiffening Effect of the FRP Panel

Despite the fact that there is an obvious buckling behaviour for the control specimen as can be seen from its buckling curve, see Fig. (12); no obvious buckling load could have been estimated from the buckling curves for the other 12 strengthened specimens. This is why there are no values stated for the buckling load in Table 4.

For further investigation of the buckling load and to address the problem of the initial slack in the curves due to the minor slippage at the initial loading stage as mentioned above, the buckling curves were reproduced; see Fig. (15). The two axes in Fig. (15) were transferred into dimensionless ones. For the load axis, this was done by dividing the applied load by the corresponding shear yielding load using Mises criteria where the yielding shear stress can be taken equal to ($f_y/\sqrt{3}$). For the displacement axis, this was performed by dividing the out-of-plane displacement by a limiting displacement (which is believed to be the limit where the behaviour of the curves turns into non-linear). The value of 1.0 mm is chosen as this limit because it represents the average limit between linear and non-linear parts in all the tests.

In Fig. (15), the slack caused by the abovementioned minor slippage was treated by drawing a hypothetical parallel curve removing this problem, as can be seen from the dashed line in the figure.

Looking at Fig. (15), it can be stated that the proposed strengthening technique is effective enough to alter the problem from an Eigen problem with respect to the control steel plate where bucking is a sudden phenomenon followed by the formation of the diagonal tension field, to a typical composite section plate where no sudden buckling is taking place anymore and the deformation process is progressing in a more stable manner.

The above discussion could be justified by the fact that the compression diagonal is not losing its capability in resisting the compression force induced by the applied shear load beyond buckling anymore because the bonded FRP panel is stiffening the steel plate along its compression diagonal. This is a unique case where the design is taking optimum advantage from both the steel plate and the strengthening FRP panel because of the biaxial action where the steel-FRP composite section is forming a composite strut resisting the compression force along the compression diagonal leaving the steel plate alone resisting the tension stress in the perpendicular diagonal. This is due to the fact that, usually, steel does not need strengthening in tension.

The FRP panel is designed to be stiff with respect to its axial direction and weak from its transverse secondary axis, this will allow the FRP panel to act like an accordion where it allows the steel plate to extend with respect to its tension diagonal without having to debond

582 and at the same time stiffening the compression diagonal of the plate. This is one of the most
583 important reasons that justify why there is no debonding between the steel plate and the FRP
584 panel (even with high deformation at failure stage), and how the typical ductile failure of the
585 steel plate is not only maintained but even improved as will be seen later in this section.
586 Another important observation is that the tension field will act as bracing force for the
587 composite compression strut in the central area leading to more buckling resistance. This
588 means that with the proposed strengthening technique we have both the advantage of the
589 composite strut resisting the compression force and the biaxial action of the steel plate in
590 resisting the shear stress at the same time.
591 However, the stiffness of the strengthened specimens is obviously much higher than the
592 control one and this need to be quantified. To do so, a relative stiffness increase index is
593 introduced. This stiffness index can be explained by looking at Fig. (15-a), the shaded area
594 between the vertical axis (the load axis) and the modified bucking curve was calculated for
595 the control specimen and then compared to the same area for the other strengthened
596 specimens. For the sake of comparison, this was done with a load equals the ultimate load of
597 the control specimen (140.0kN). The stiffness index then can be written as
598
599 $$S.I = Act / Ast \quad \text{.....(2)}$$
600
601 where:

S.I: is the relative stiffness increase index,

Act: is the shaded area between the vertical axis (the load axis) and the modified bucking curve for the control specimen,

Ast: is the shaded area between the vertical axis (the load axis) and the modified bucking curve for the strengthened specimens, up to a load equal to 140 kN.

602
603 Another important property that needs to be quantified as well is the change in energy
604 absorption capacity (ductility) of the specimens. Usually the increase in the capacity of the
605 strengthened specimen comes at a considerable reduction in the energy absorption (Okeil et
606 al, 2009). In this study, the proposed strengthening technique is targeting the out-of-plane
607 displacement while limited and insignificant effect is observed with the deflection curves.
608 This will lead to the controversial question whether we should use the deflection curves or
609 the buckling curves to estimate the energy absorption capacity. However, this is not the core

610 of this study; therefore a simple relative energy absorption index is proposed to compare the
611 ductility of the strengthened specimens with the control one.
612 The increase in energy absorption factor can be taken as the area between the horizontal axis
613 (the displacement axis) and the modified buckling curve of the strengthened specimen
614 divided by the same area for the control specimen, see Fig. (15-a). The limit of 10mm was
615 chosen to be the basis of comparison because most of the tested specimens reached this
616 value; however, the ones who were stopped before this limit for technical reasons were
617 extended to an out-of-plane displacement equals 10mm. Thus, the relative energy absorption
618 index can be stated as:
619
620 $E.I = Asb / Acb$ .....(3)
621
622 where:

E.I: is the relative energy absorption index,

Asb: is the area between the horizontal axis (the displacement axis) and the modified buckling curve for the strengthened specimens,

Acb: is the area between the horizontal axis (the displacement axis) and the modified buckling curve for the control specimen.

623
624 Table 5 illustrate the values both for the relative stiffness and energy absorption indices. It
625 can be seen that the proposed strengthening technique succeeded in increasing the stiffness 3
626 times and that was not on the expense of energy absorption as it is improved up to 50%. It is
627 worth mentioning that these two factors were not calculated for specimens with irregular
628 buckling curves where the mode of buckling is altered (i.e. SP-8, SP-10, and SP-12).
629

630 **NUMERICAL MODELLING**

631 A non-linear finite element model was used to model the test specimens. These preliminary
632 models are meant to act as indicators and bench marks for the tested specimens and to prove
633 the validity of the proposed picture-frame testing rig; rather than an accurate finite element
634 simulation to be used for a parametric study in the future. More accurate models shall be
635 presented in a separate paper for the cyclic series of tests. Commercial software (*Abaqus*
636 6.10) was used. The steel plate and the FRP panel were modelled using a nine node reduced
637 integration shell element S9R5, which have five degrees of freedom per node. This element is
638 not available in *Abaqus* standard CAE and can be used only through an *Abaqus* input file.

S9R5 elements are meant for slender plates and were derived originally according to Kirchhoff thin plate bending theory. A Matlab code was written to create the nodes and element incidences to be incorporated in *Abaqus* input files. The size of the web elements was chosen to be 20×20mm based on the aforementioned convergence study. The initial imperfection was found using the elastic Eigen buckling modes; these were initiated using the buckling analysis available in *Abaqus CAE* and then imposed as an initial imperfection using *Abaqus* script commands in the input file.

A bilinear elasto-plastic stress-strain curve was adopted for the steel constitutive model, with a modulus of elasticity (E_s) of 200GPa and yield strength (f_y) of 275MPa. The FRP constitutive material model was simply an equivalent isotropic shell section with a modulus of elasticity of 22.1GPa and 43.9GPa for the GFRP and the CFRP, respectively. Tie constraints are applied between the steel plate and the FRP bonding strips for simplicity, even though it is known that tie constraint will give higher capacity than the same model with cohesive surface interaction instead.

Due to the numerical analysis time cost of the original picture-frame finite element model (Fig. 10-b), which takes usually between 24 to 36 running hours on a core i7 laptop; a simplified model was adopted in this paper, see Figs. (16-a) and (16.b). In Fig. (16-c) the implemented boundary conditions are shown. Table 6 illustrates these boundary conditions in detail. The simplified model is basically the steel plate tied to a surrounding plate frame with an optimized stiffness to simulate the original one. The four corners' hinges were simulated by coupling the translational displacements and freeing the rotational ones. The picture-frame plates were modelled using S4R elements available in *Abaqus CAE*. The loads were applied as shown in Fig. (15-a) and (15-b) to provide the pure shear status and to make sure that the model works properly.

Fig. (17) shows that the model predicts both the strength and the behaviour of the control specimen (without FRP strengthening) with reasonable accuracy. However, the composite model does not show the same accuracy. This may be mostly attributed to the above mentioned slack that took place during the test due to the minor slip at the top left corner of the picture-frame along the diagonal tension field. This took place because there was no mechanical anchorage between the plate and the picture-frame and the grip was solely dependent on the friction according to the original design. This problem was solved in the cyclic series of tests by using a different testing mechanism. Nevertheless, the composite model predictions are acceptable as indicators and not as reference values.

673 ## CONCLUSIONS

674 A novel preformed corrugated FRP panel is introduced in this study to strengthen slender
675 steel plates, such as the web of a plate girder, against breathing deformations of plates leading
676 to fatigue failures. The section of the FRP panel was optimized using finite element
677 modelling accounted for minimizing the cost of the FRP material, the quantity of adhesive
678 being used, workmanship, and the complexity of the multi-axial stress state in the web steel
679 plate.

680 The subsequent study was divided into five phases. Phase-1 involved optimizing the new
681 strengthening technique through finite element modelling. Phases-2 and -3 involved choosing
682 the adhesive and determining the material mechanical properties for the FRP used through
683 DLS and tension specimens, respectively. Phase-4, which is named the 'initial' series in this
684 paper, was performed to test the efficiency of the proposed panel under static loading.
685 Thirteen steel plates were strengthened with the proposed preformed corrugated FRP panel
686 and tested using a special picture-frame rig. This was designed to hold the steel plate in
687 position with the required boundary conditions while applying in-plane shear without the
688 need to weld the plate into a stiff frame like the case with ordinary plate girders.

689 The results of the initial series of tests proved the efficiency of the proposed strengthening
690 technique in increasing the stiffness of the steel plate section up to 3.0 times that of the
691 unstrengthened one and consequently increasing its buckling shear stress. In addition to that,
692 the proposed strengthening technique succeeded in preserving the ductile prototype failure
693 associated with intact (unstrengthened) steel plate girders, which is a very important factor in
694 safety usually ignored by other FRP strengthening techniques. As a matter of fact the energy
695 absorption capacities of the strengthened specimens have been shown to exceed that of the
696 unstrengthened ones by a factor of 1.5. No bonding failure could be detected during or after
697 the test even when the steel plate was highly deformed and fully yielded.

698 The variables studied in this series were, (1) the effect of FRP material which significantly
699 affected the stiffness and buckling behaviour of the strengthened specimens. The CFRP
700 showed more superior behaviour in increasing the stiffness and the shear buckling stress of
701 the strengthened specimens due to its higher modulus of elasticity than the GFRP; (2) the
702 type of section (open versus closed), which showed no significant effect in increasing the
703 stiffness and bonding capacity with respect to the originally proposed open section one; (3)
704 the number of the FRP layers used to make the corrugated panel had a significant effect on
705 the behaviour of the strengthened specimens where the 3-layered ones showed higher
706 capacity and much more stable and ductile behaviour especially for the GFRP ones; (4) the

orientation of the GFRP used, which was taken with respect to the corrugation axis, had a moderate effect on the behaviour of the strengthened specimens. The 0°-90° succeeded in slightly increasing the ultimate strength for the 3-layered specimen while it altered the mode of failure to a more brittle one with respect to the 2-layered one; (5) The effect of the end cut of the FRP panel wasn't very significant in comparing type A (i.e. the triangular cut) and B (i.e. the circular cut) where they almost acted the same but was significant for type C (i.e. the long one) even when the mode of failure was altered for the GFRP specimen. This is believed to be due to the longer dimension which provided less stiffness to the panel and consequently may alter the mode of failure form an even buckling mode (for an aspect ratio of 1.0) to an odd one.

A geometrical and material non-linear analysis was used to model the specimens in this study. A simplified picture frame model was utilized in this study to avoid the more numerically expensive original model. The unstrengthened model was able to realistically simulate the behaviour of the specimens throughout all loading stages, while the strengthened model provided convincing results only up to the failure plateau.

ACKNOWLEDGMENTS

This work was sponsored by the Ministry of Higher Education and Scientific Research in Iraq. The School of Engineering at the University of Edinburgh, which is part of the Edinburgh Research Partnership in Engineering (ERPE), is acknowledged for providing support to this project.

REFERENCES

- Al-Azzawi, Z., Stratford, T., Rotter, M., and Bisby, L., "FRP Shear Strengthening of Thin-Walled Plate Girder Web Panels Subjected to Cyclic Loading", Proceedings of PROTECT 2015, fifth international workshop on performance, protection & strengthening of structures under extreme loading, East Lansing, MI, USA, June 2015, pp. 350-359.
- Assoodani, Firas Abdul-Razzaq; "Shear behaviour and strength of CFRP retrofitted steel plate girders and steel-concrete composite plate girders", PhD thesis, University of Technology, Iraq, July 2014, 610 pp.
- Bhutto, Muhammad Aslam. "FRP composites for strengthening of steel bridge members," Proceedings of the 15th young researchers' conference, 14 March, 2013.
- Bureau of Transportation Statistics. "Transportation statistics annual report 2008," United States Department of Transportation, Research and Innovative Technology Administration, USA, 2008. National Bridge Inventory Database (NBI), Federal Highway Administration, Wikipedia, https://en.wikipedia.org/wiki/National_Bridge_Inventory.
- Miyashita T., Okuyama Y., Nagai M., Wakabayashi D., Koide N., Hidekuma Y., Kobayashi A., Horimoto W., "Shear buckling tests of steel girder bonded carbon fiber reinforced plastic on its web", Structural faults and repair, Edinburgh, 2012.
- Okeil, A.M., Bingol, Y., and Ferdous, Md.R. " Novel technique for inhibiting buckling of thin-walled steel structures using pultruded glass FRP sections", Journal of Composites for Construction, 13(6), 2009, pp. 547-557.

- Patnaik A.K. and Bauer, C.L. “Strengthening of Steel Beam with Carbon FRP Laminates”, Proceedings of the 4th International Conference on Advanced Composite Materials in Bridges and Structures, Calgary, July 2004.
- Roberts, T. M., Davies, A. W., and Bennett, R. J. H., “Fatigue shear strength of slender web plates”, Journal of Structural Engineering, October 1995, pp. 1369-1401.
- Roberts, T. M., Osman, M. H., Skaloud, M. and Zornerova, M., “Fatigue crack propagation and residual strength of slender web panels”, International Colloquium on Stability of Steel Structures, Budapest, 1995.
- Skaloud, M. and Zornerova, M. “The fatigue behaviour of the breathing webs of steel bridge girders,” Journal of Civil Engineering and Management, Vol. XI, No. 4, 2005, PP. 323-336.
- Schnerch, D.A. “Strengthening of steel structures with high modulus carbon fibre reinforced polymer (CFRP) materials,” PhD Thesis, North Carolina State University, 2005, 265 pp.

List of Tables:

Table Ref.	Caption
Table 1	Manufacturers’ fibre properties
Table 2	Double shear lap test series results*
Table 3	Mechanical and geometrical properties of FRP used in this study
Table 4	Test variables
Table 5	Increase in stiffness and energy absorption indices for the initial series
Table 6	Simplified picture frame model boundary conditions

List of Figures:

Figure Ref.	Caption
Fig. 1	Schematic showing shear buckling wave parallel to the tension diagonal, and the FRP strengthening panel used in this work parallel to the compression diagonal.
Fig. 2	Analytical model adopted in this study
Fig. 3	Composite section profile and sectional dimensions
Fig. 4	Critical buckling shear stress versus the inverse of the degrees of freedom
Fig. 5	Finite element model of classical and proposed strengthening techniques
Fig. 6	Position, section, and end cut shape of FRP panels used in Phase 3
Fig. 7	Front and side views of typical double lap shear specimen
Fig. 8	DSL and Tension tests
Fig. 9	Preformed CFRP corrugated panel and vacuum bagging consumable materials
Fig. 10	Picture frame analogy
Fig. 11	Specimen details and test instrumentations
Fig. 12	Out-of-plane displacement curves for phase-4 tests
Fig. 13	Photos for specimens after test- Phase-4
Fig. 14	Load-Deflection Curves
Fig. 15	Dimensionless buckling curves
Fig. 16	Simplified picture frame finite element model
Fig. 17	Verification curves of the simplified picture frame model

772
773 Table 1: Manufacturers' fibre properties

	PYROFIL TR50S 12K carbon fibre	Glass fibre
Tensile strength (MPa)	4900	2200
Tensile modulus (GPa)	240	80
Ultimate elongation (millistrain)	-	3.5
Typical density g/cm^3	1.82	2.6
Fibre mass per unit length (mg/m)	800	-

774
775
776
777
778
779
780 Table 2: Double shear lap test series results
781

Specimen	Load, kN	Stress, MPa
GFRP-600-ES	6.47	5.38
CFRP-650-ES	11.82	9.83
GFRP-600-TS	8.25	6.86
CFRP-650-TS	12.39	10.3
GFRP-600-EE	4.47	3.94
CFRP-650-EE	9.15	7.61
GFRP-600-TE	5.46	4.54
CFRP-650-TE	8.77	7.29
GFRP-600-ET	3.03	2.52
CFRP-650-ET	6.8	5.66

- The first 4 letters stands for glass or carbon fibre reinforced polymer.
- The numbers stands for the weight of the fabric g/m^2.
- The last 2 letters stands for the resin used, E for EL2, T for Tyfo, and S for Sikadur-330. While the order of them specifies which one of them is the saturating resin and which one is the bonding epoxy, as the first stands for the saturating resin and the second goes for the bonding epoxy.

782
783
784
785
786
787 Table 3: Mechanical properties of the FRP used in this study

Specimen	FVF	F_f, MPa	ε_f	E_f, GPa	Note
CFRP-650	0.58	527.66	0.28	32.23	2-Layers
CFRP-450	0.59	704.513	0.22	48.12	3-Layers
GFRP-600-45°-45°	0.49	34.45	0.50	7.35	2-Layers
GFRP-440-45°-45°	0.48	61.57	-	18.02	3-Layers
GFRP-600-0°-90°	0.49	238.56	0.52	18.71	2-Layers
GFRP-440-0°-90°	0.48	294.14	0.72	14.34	3-Layers

788
789
790
791
792
793
794
795

796 Table 4: Test variables

Ref.	Specimen	FRP type	Panel type	No. of layers	Fibre orientations*	Buckling load, kN	Ultimate load, kN
SP-1-4	Control Specimen	-	-	-	-	≈ 40.0	140.0
SP-2	GFRP-600-2L	Glass	Type A	2-Layers	+45°/-45°	-	147.8
SP-3	CFRP-650-2L	Carbon	Type A	2-Layers	0°/90°	-	160.5
SP-4	GFRP-600-2L-Closed	Glass	Type A	2-Layers	+45°/-45°	-	149.3
SP-5	CFRP-650-2L-Closed	Carbon	Type A	2-Layers	0°/90°	-	165.0
SP-6	GFRP-440-3L	Glass	Type A	3-Layers	+45°/-45°	-	157.0
SP-7	CFRP-450-3L	Carbon	Type A	3-Layers	0°/90°	-	153.3
SP-8	GFRP-600-2L-0-90	Glass	Type A	2-Layers	0°/90°	-	155.1
SP-9	GFRP-440-3L-0-90	Glass	Type A	3-Layers	0°/90°	-	155.3
SP-10	GFRP-600-2L-B	Glass	Type B	2-Layers	+45°/-45°	-	161.3
SP-11	CFRP-650-2L-B	Carbon	Type B	2-Layers	0°/90°	-	166.2
SP-12	GFRP-600-2L-C	Glass	Type C	2-Layers	+45°/-45°	-	153.0
SP-13	CFRP-650-2L-C	Carbon	Type C	2-Layers	0/90	-	173.8

797 * The orientation here is taken with respect to the corrugation axis.

798

799 Table 5: Increase in stiffness and energy absorption indices for the initial series

Ref.	Specimen	Stiffness index	Energy absorption index
SP-1-4	Control Specimen	1.0	1.0
SP-2	GFRP-2L-(45°-45°)-A	1.4	1.1
SP-3	CFRP-2L-(0°-90°)-A	2.9	1.4
SP-4	GFRP-2L-(45°-45°)-A-Closed	1.6	1.2
SP-5	CFRP-2L-(0°-90°)-A-Closed	2.6	1.4
SP-6	GFRP-3L-(45°-45°)-A	1.8	1.2
SP-7	CFRP-3L-(0°-90°)-A	3.0	1.3
SP-8	GFRP-2L-(0°-90°)-A	-	-
SP-9	GFRP-3L-(0°-90°)-A	1.6	1.2
SP-10	GFRP-2L-(45°-45°)-B	-	-
SP-11	CFRP-2L-(0°-90°)-B	2.7	1.4
SP-12	GFRP-2L-(45°-45°)-C	-	-
SP-13	CFRP-2L-(0°-90°)-C	3.2	1.5

800

801

802 Table 6: Simplified picture frame model boundary conditions

Surface	u	v	w	θ_x	θ_y	θ_z
1	1	1	1	1	1	0
2	0	0	1	1	1	0
3	1	1	1	1	1	1
4	0	0	1	1	1	1

803 **1**: *stands for fixed and* **0**: *stands for free*

804

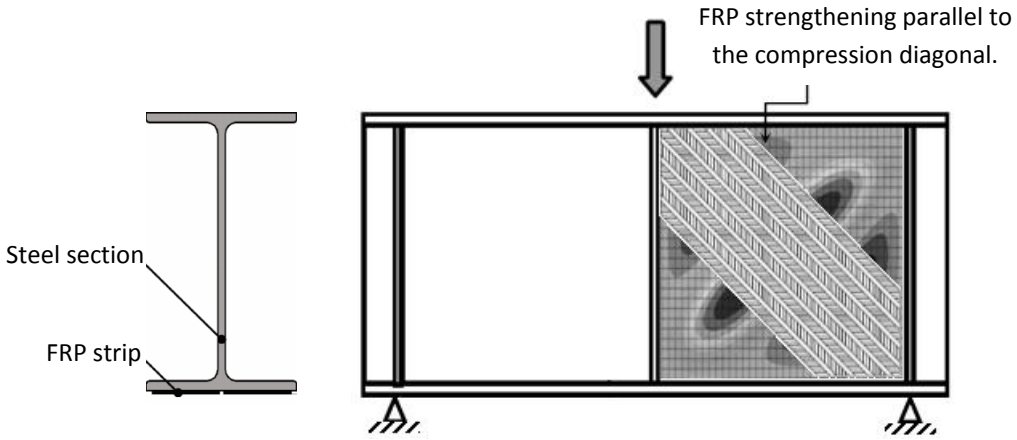

(**a**) FRP Flexural Strengthening (**b**) Proposed FRP strengthening against shear buckling

Fig. (1): Schematic showing the proposed strengthening technique compared to a typical flexural FRP strengthening.

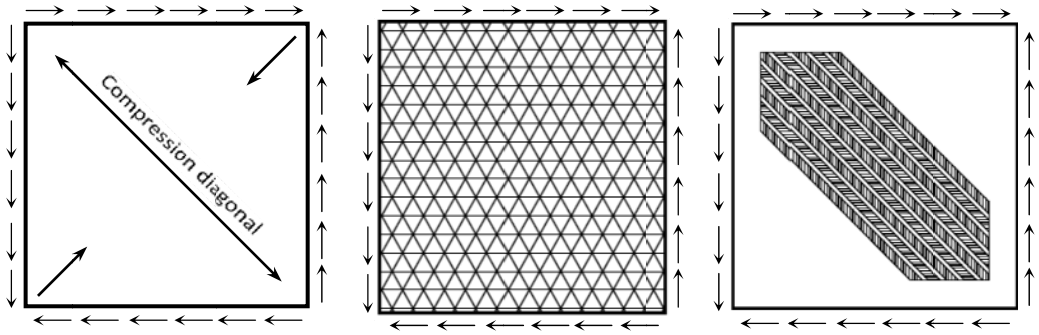

(**a**) Initial steel (**b**) Classical model (**c**) Proposed model

Fig. (2): Analytical model adopted in this study.

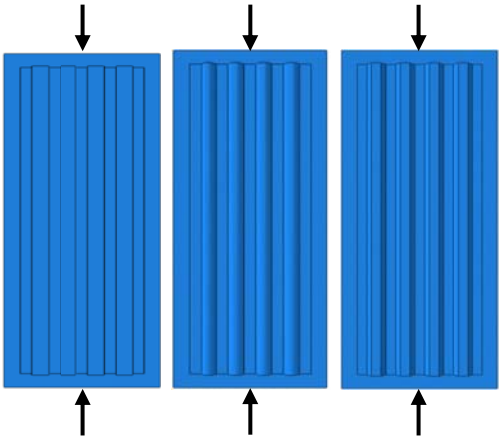

(**a**) Composite section profile

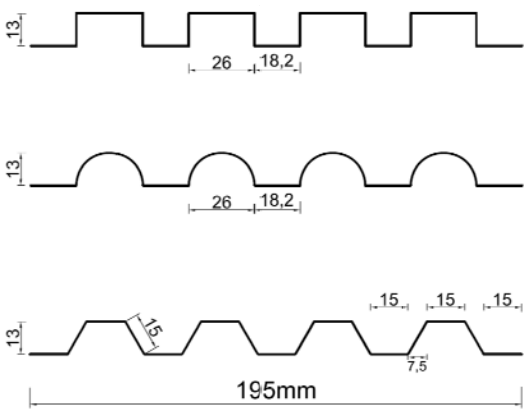

(**b**) FRP panel corrugation sections

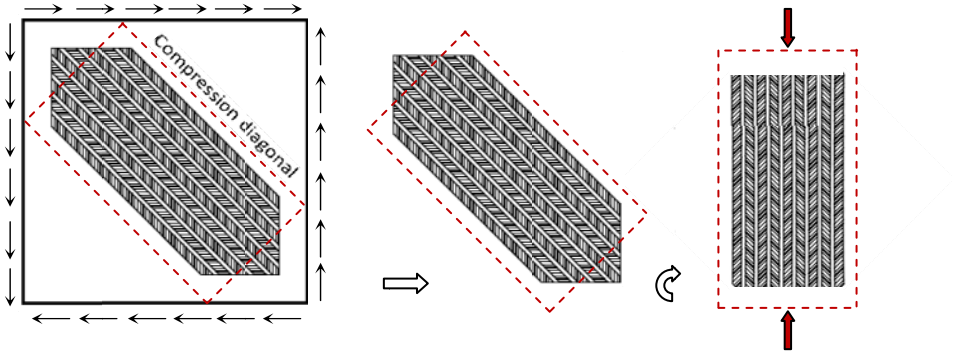

(**c**): Strengthened steel plate under pure shear stress and the compression diagonal strip used for Euler buckling analysis.

Fig. (3): Composite section profile and sectional dimensions.

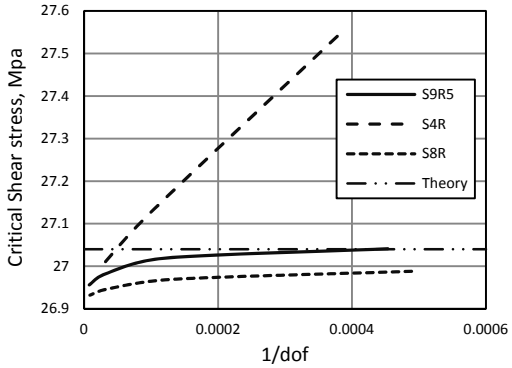

Fig. (4-a): Simply supported boundary conditions.

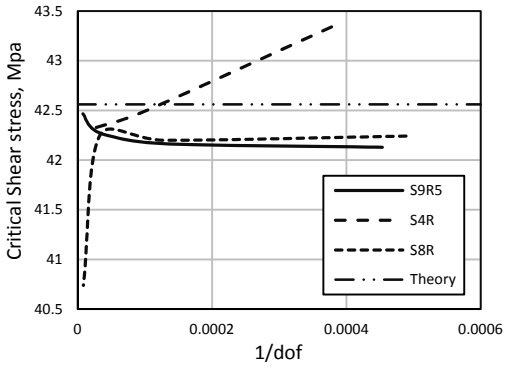

Fig. (4-b): Fixed boundary conditions.

Fig. (4): Critical buckling shear stress versus the inverse of the degrees of freedom.

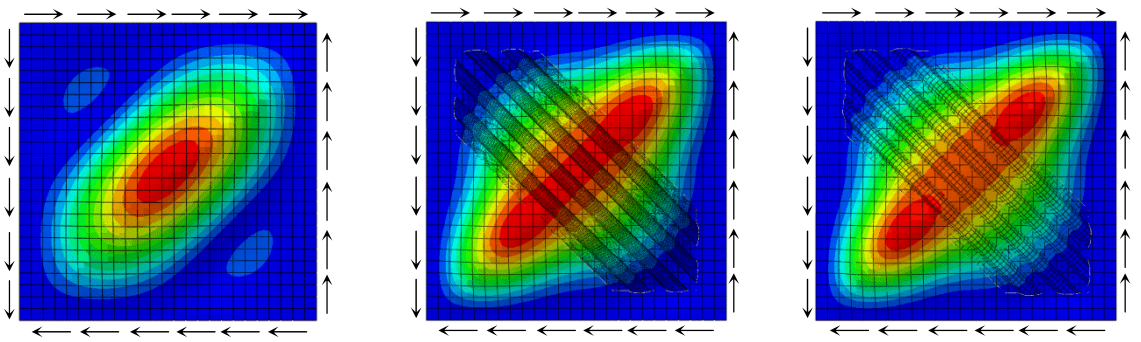

(**a**): Classical technique (**b**): Semi-circular section (**c**): Half-hexagonal section.

Fig. (5): Finite element model of classical and proposed strengthening techniques.

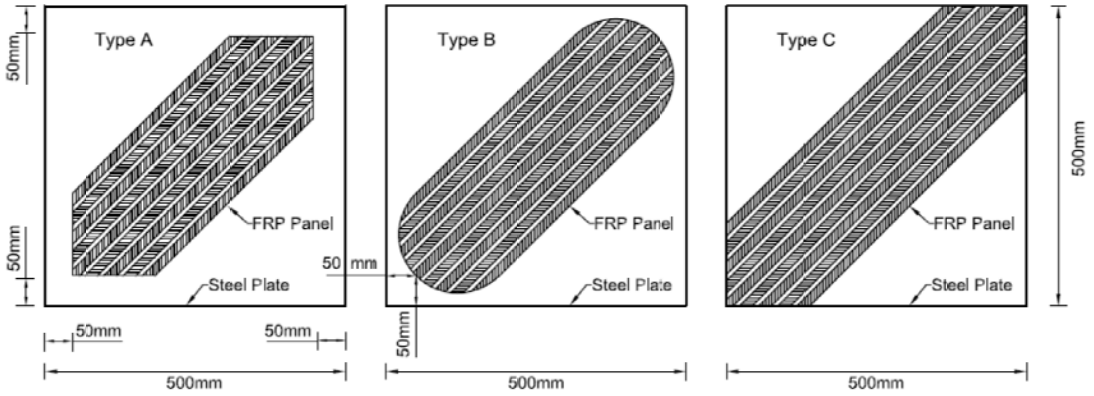

(**a**) FRP strengthening configurations

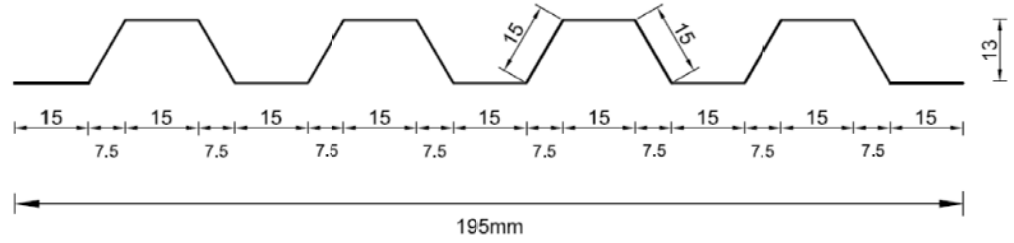

Open FRP section

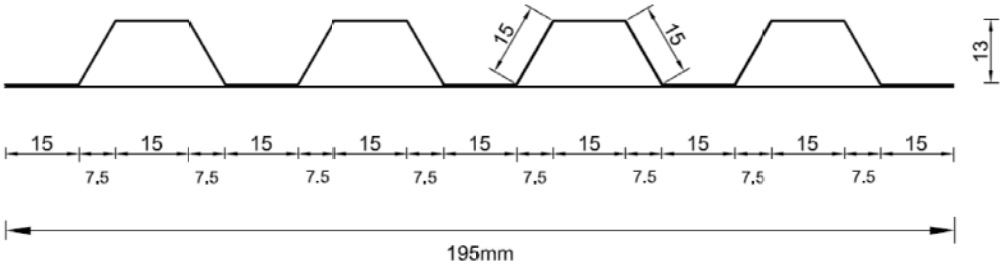

Closed FRP section

(**b**) Open versus closed FRP corrugated sections

Fig. (6): Position, section, and end cut shape of FRP panels.

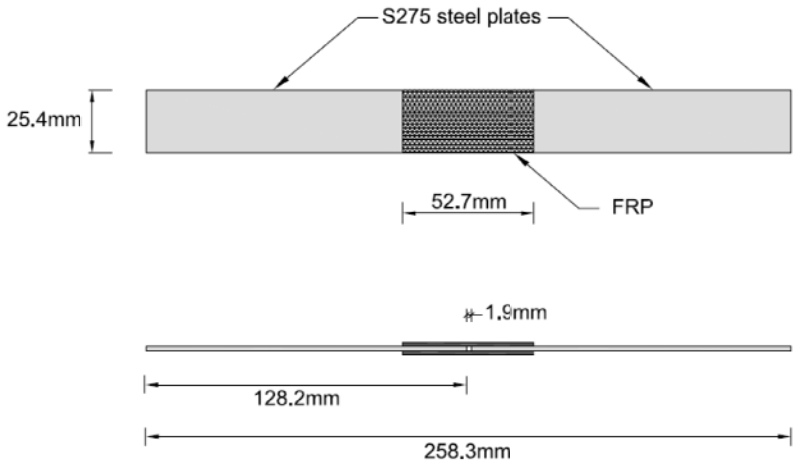

Fig. (7): Front and side views of typical double lap shear specimen.

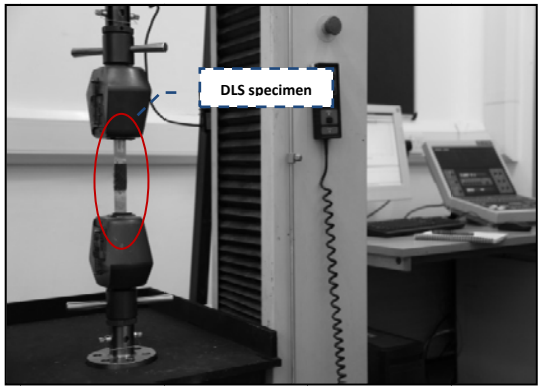

Fig. (8-a): DLS test setup.

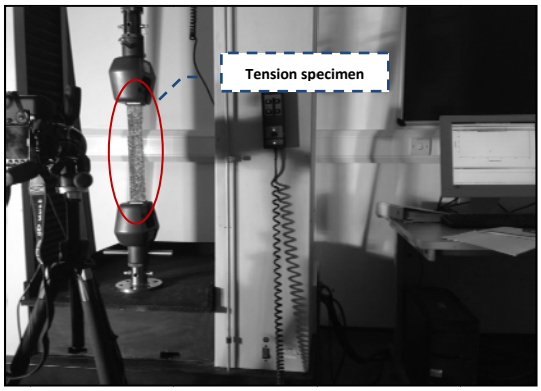

Fig. (8-b): Tension tests with DIC setup.

Fig. (8): DSL and Tension tests setup.

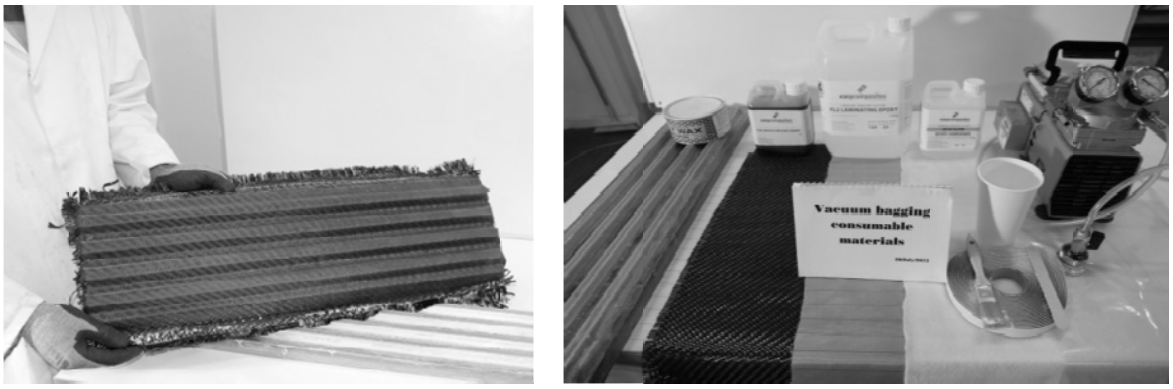

(**a**): The preformed FRP panel (**b**): Vacuum bagging consumable materials

Fig. (9): Preformed CFRP corrugated panel and vacuum bagging consumable materials.

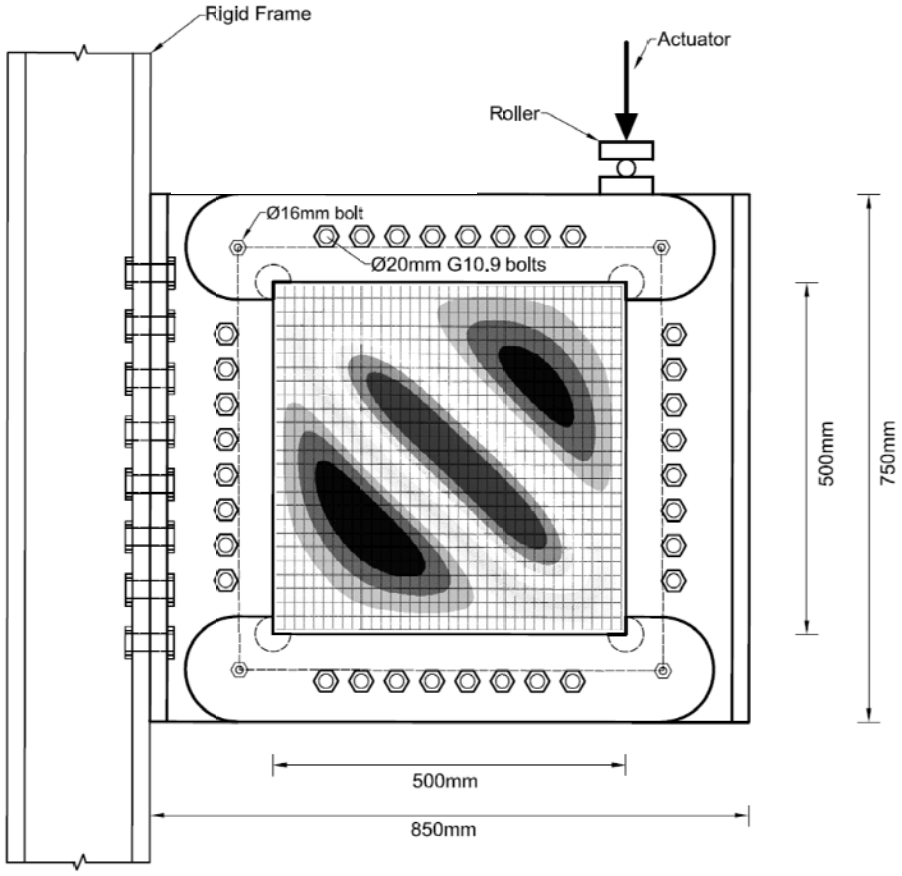

(**a**) Picture-frame diagram and details

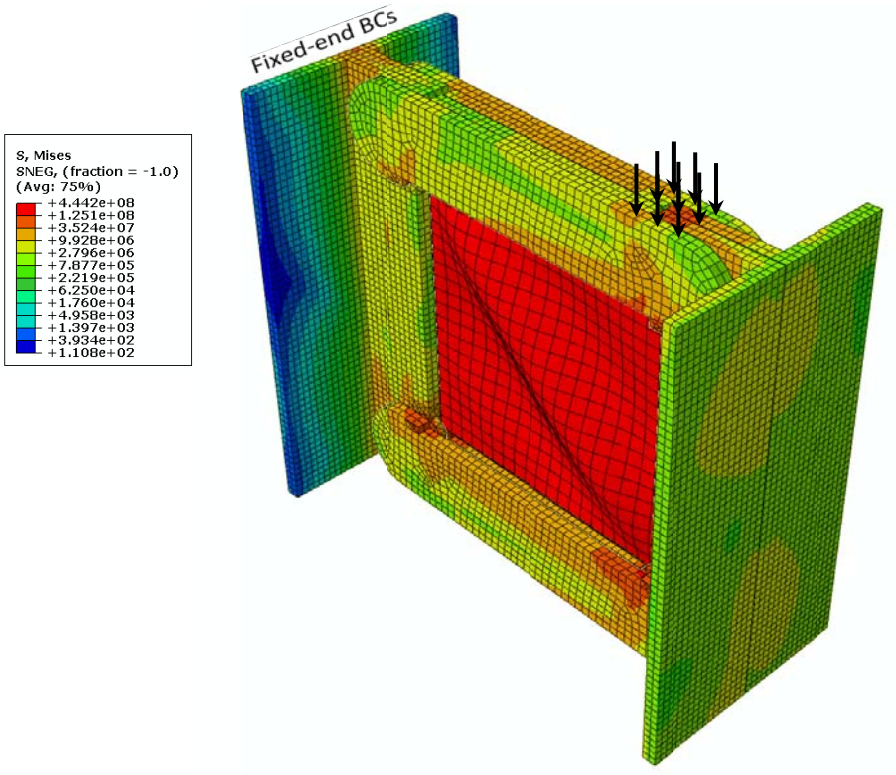

(**b**) Three dimensional visualization of logarithmic scale Von Mises stress distribution in the plate and picture-frame components (N/m^2)

Fig. (10): Picture-frame analogy.

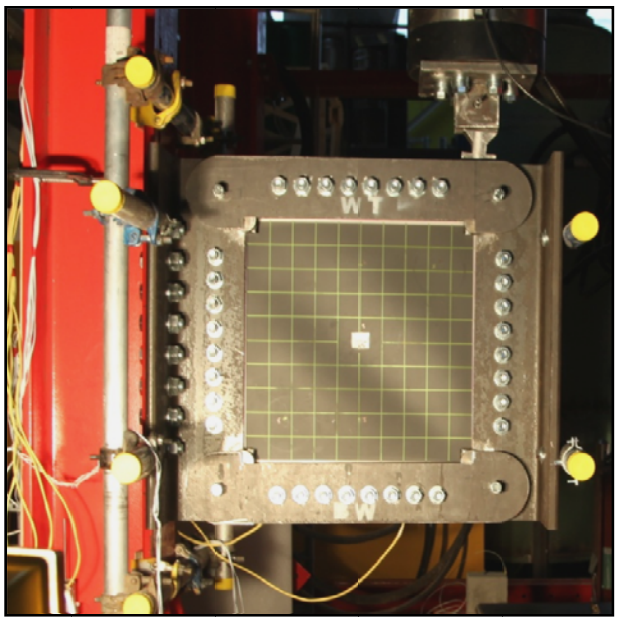

(**a**): Control specimen- front face

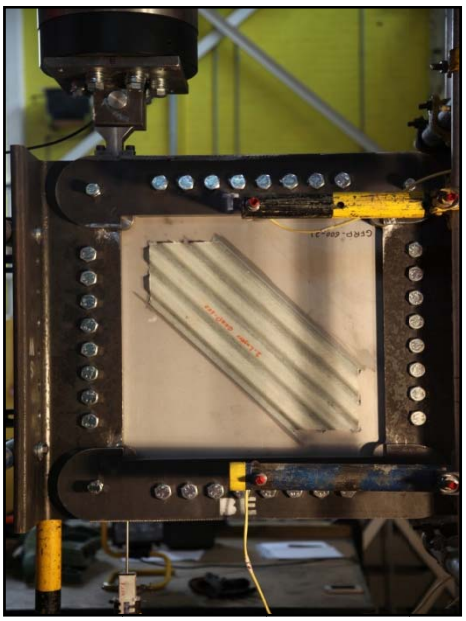

(**b**): Typical strengthened specimen- back face

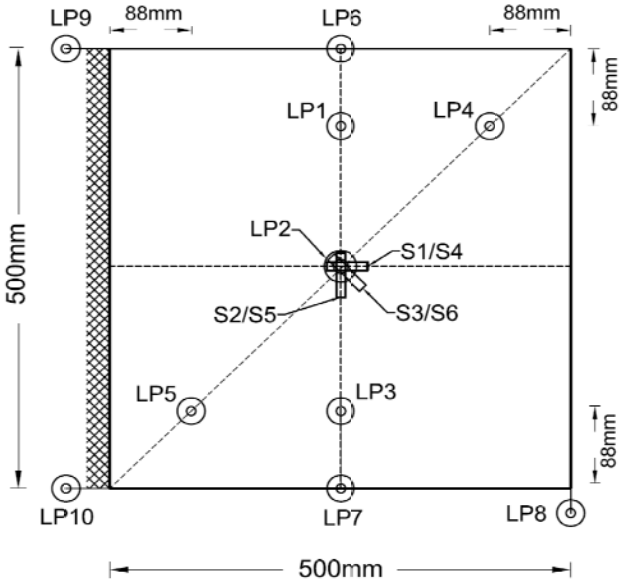

(**c**): LPs and strain gauge locations

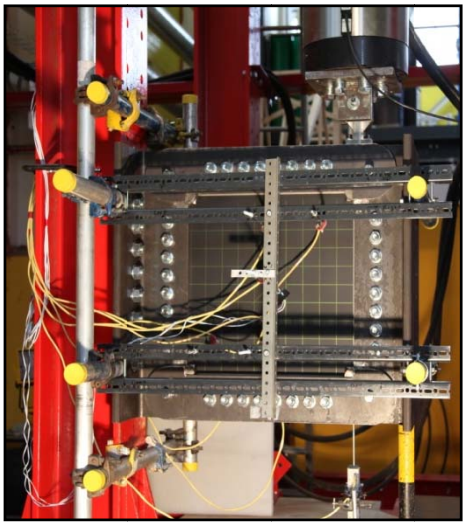

(**d**): Test instrumentations

Fig. (11): Specimen details and test instrumentations.

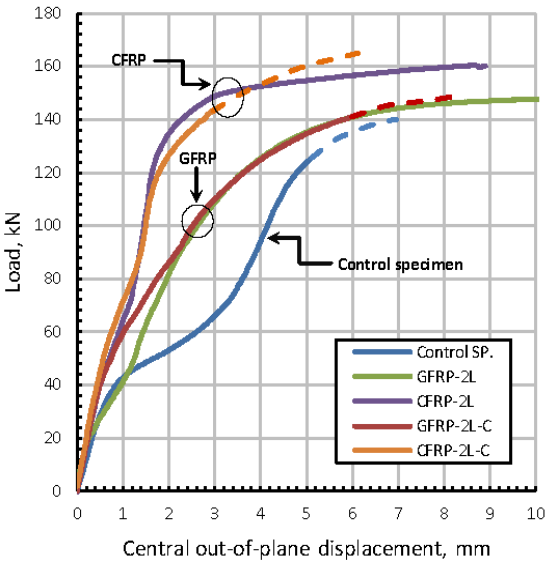

(**a**): Comparison of 2-layerd open & closed

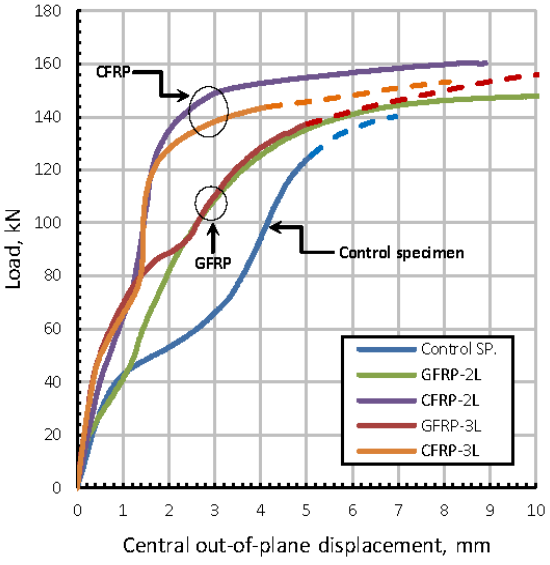

(**b**): Comparison of 2 and 3 layered open section

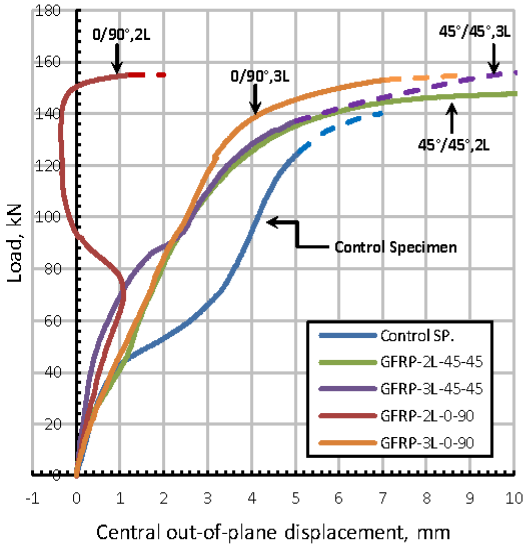

(**c**): Comparison of GFRP fibre orientations

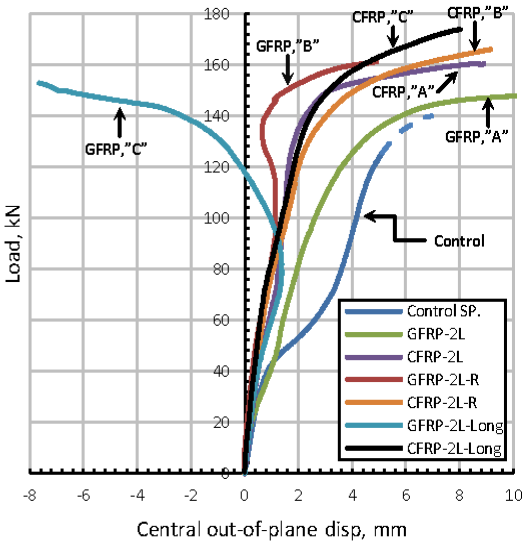

(**d**): Comparison of Type A, B, and C end cut

Fig. (12): Out-of-plane displacement curves for phase-4 tests.

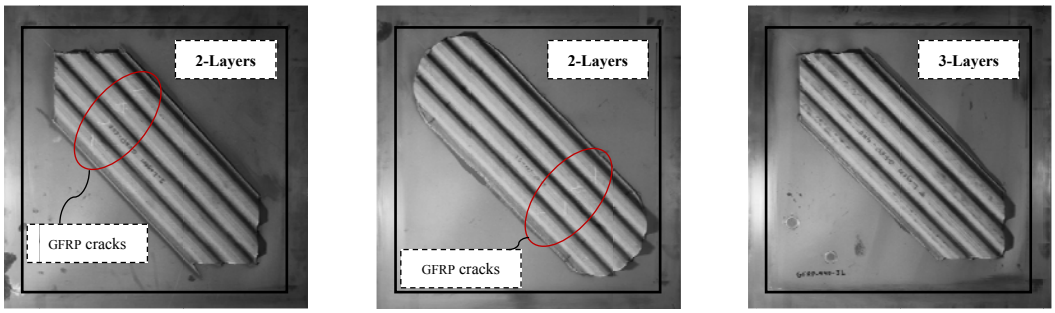

(**a**): Typical failure of GFRP strengthened specimens- Phase-4.

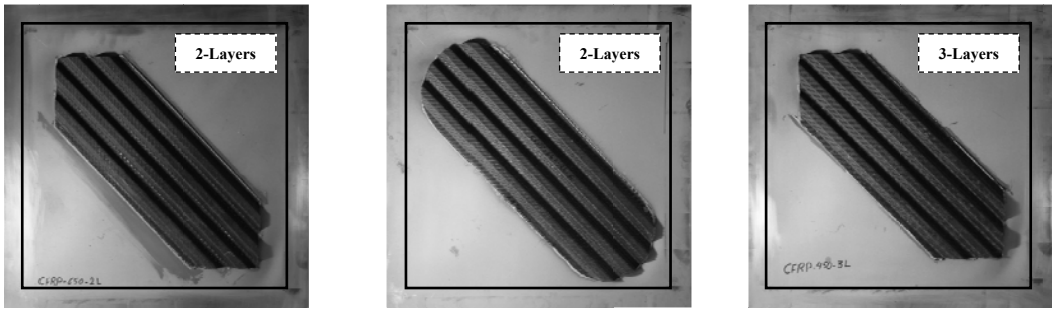

(**b**): Typical failure of CFRP strengthened specimens- Phase-4.

Fig. (13): Photos for specimens after test- Phase-4.

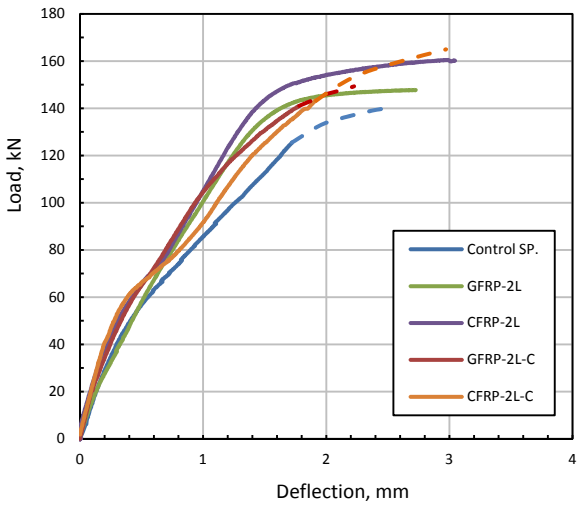

(**a**): Comparison of 2-layerd open & closed.

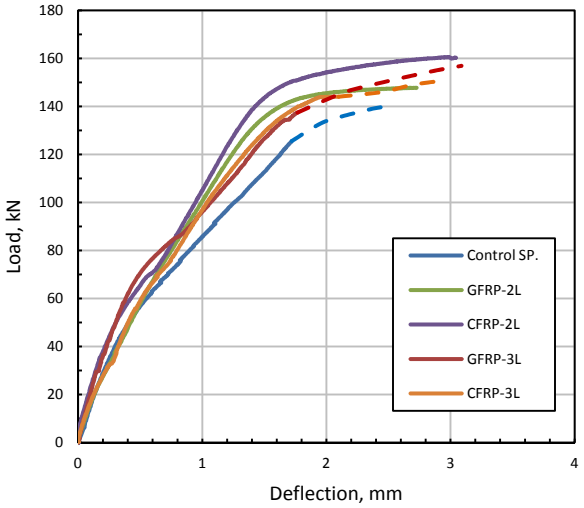

(**b**): Comparison of 2 and 3 FRP layers.

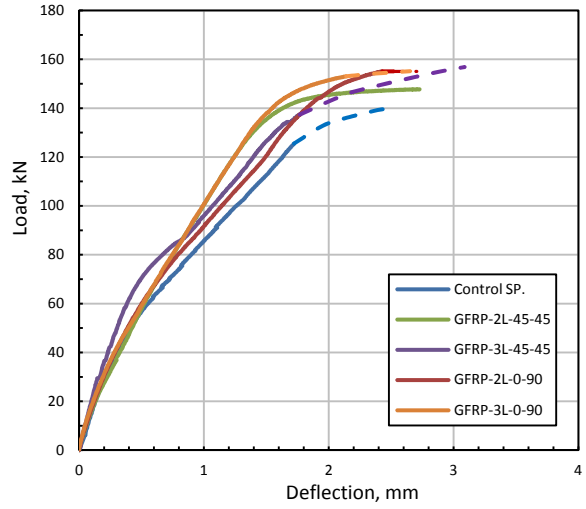

(**c**): Comparison of GFRP fibre orientations.

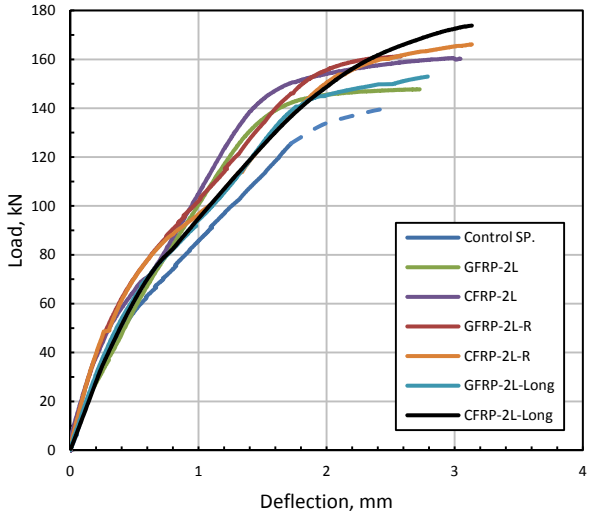

(**d**): Comparison of Type A, B, and C.

Fig. (14): Load-Deflection Curves.

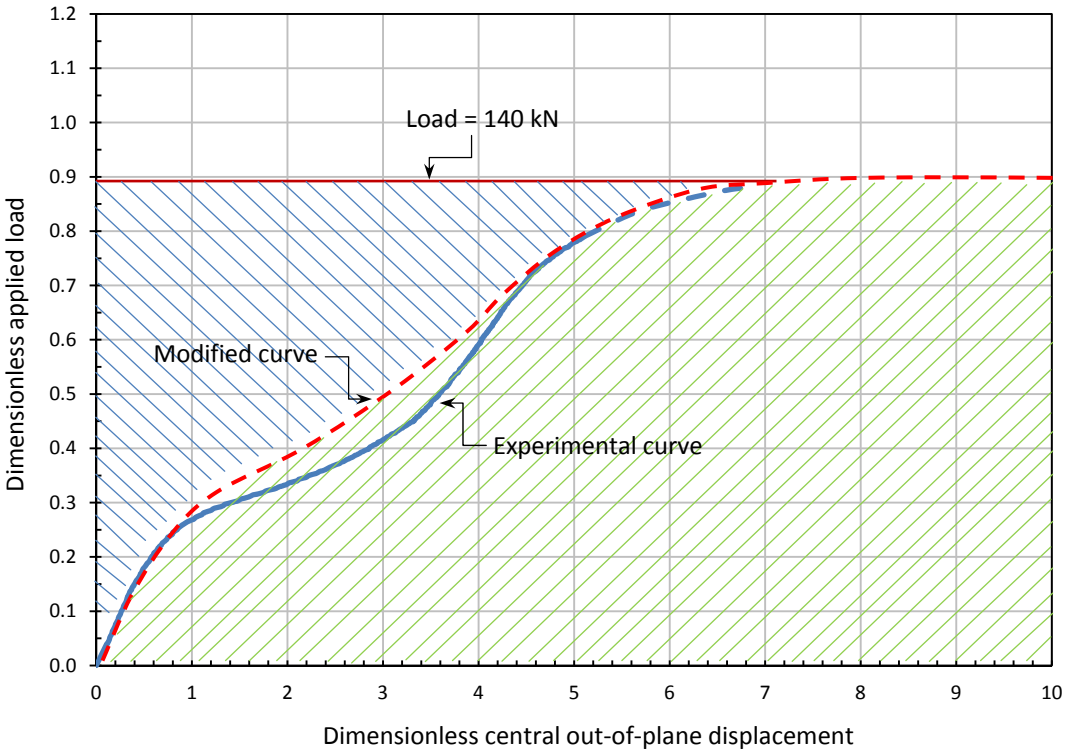

(**a**) Control specimen, SP-1.4

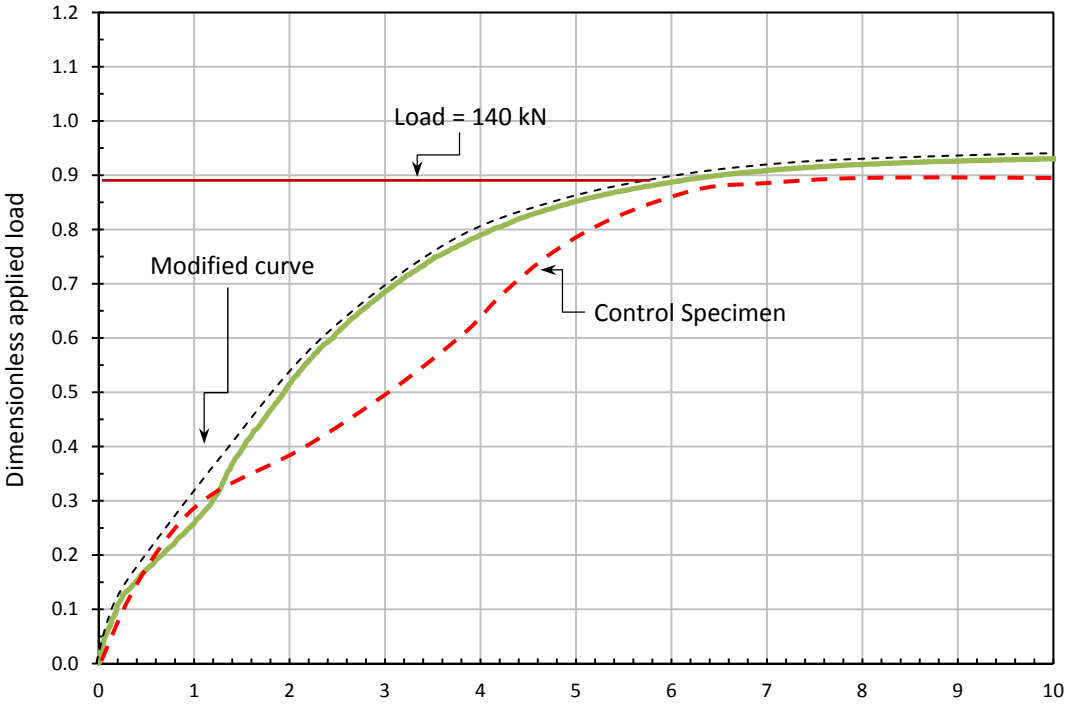

(**b**) Typical modified curve for a strengthened specimen, SP-2

Fig. (15): Dimensionless buckling curves.

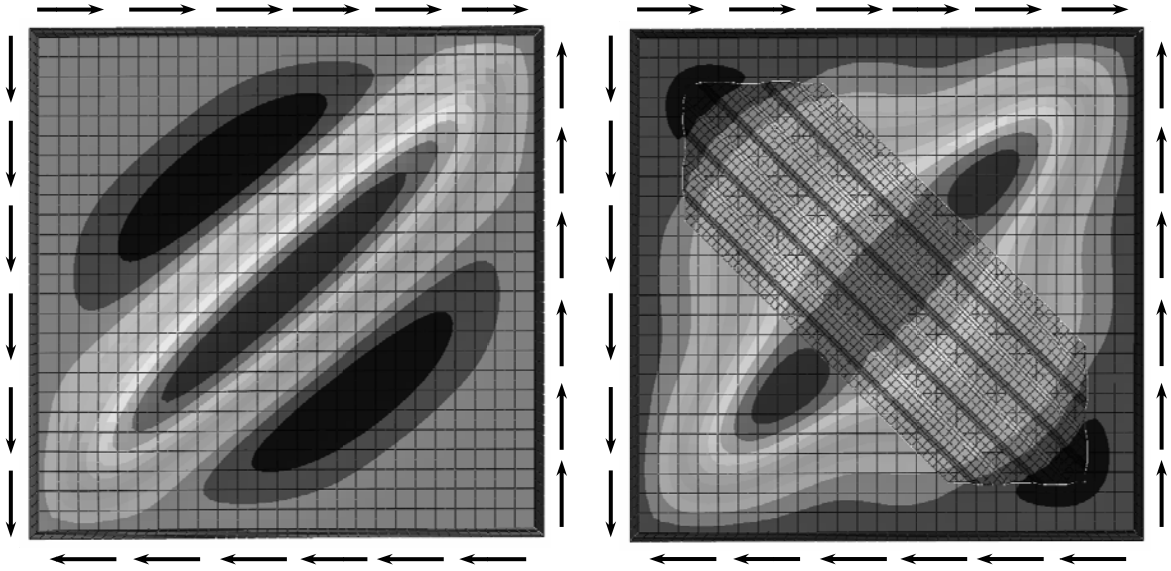

(**a**): Control model.

(**b**): FRP strengthened model.

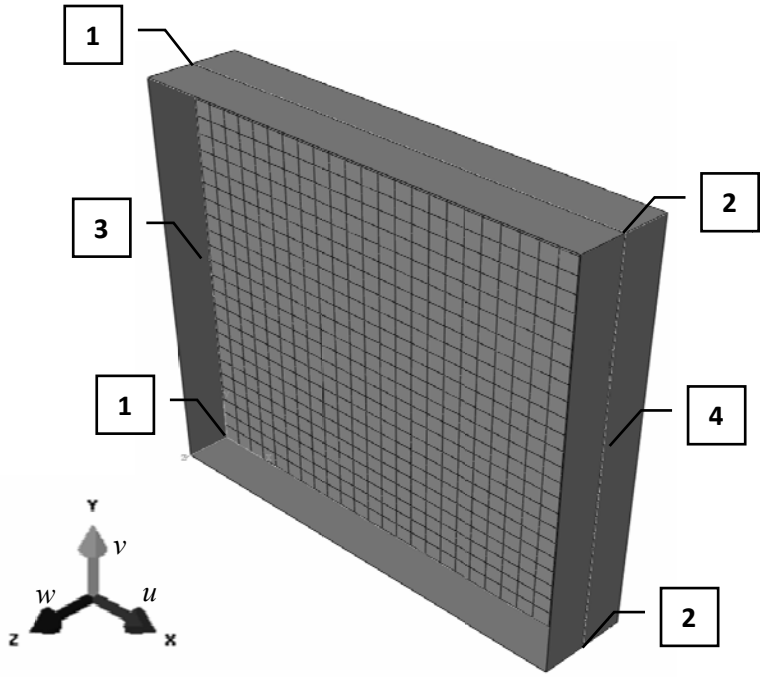

(**c**): Boundary conditions of the simplified picture frame.

Fig. (16): Simplified picture frame finite element model.

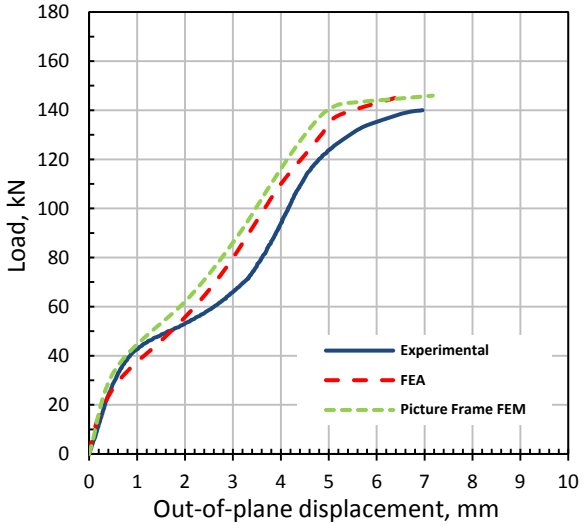

(**a**): Control specimen.

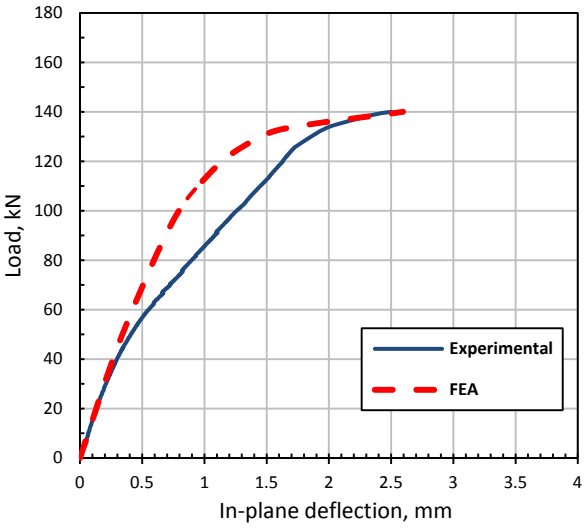

(**b**): Control specimen.

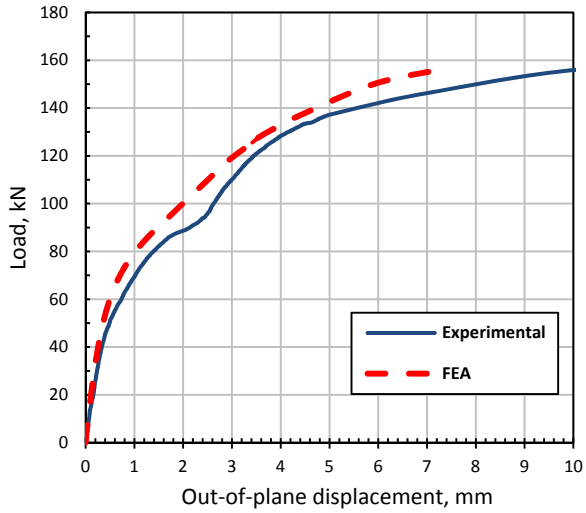

(**c**): GFRP specimen-SP-6.

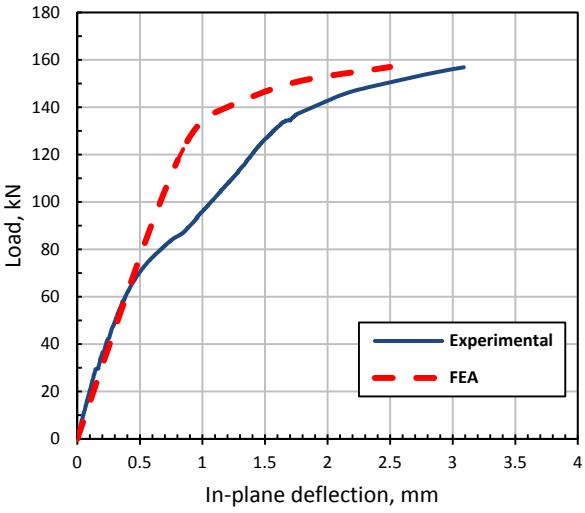

(**d**): GFRP specimen-SP-6.

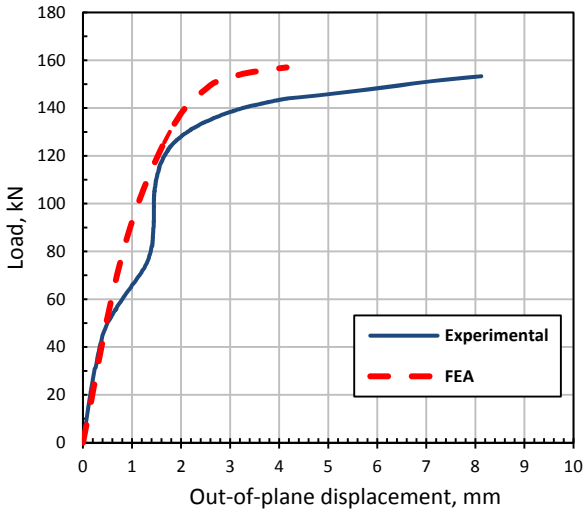

(**e**): CFRP specimen-SP-7.

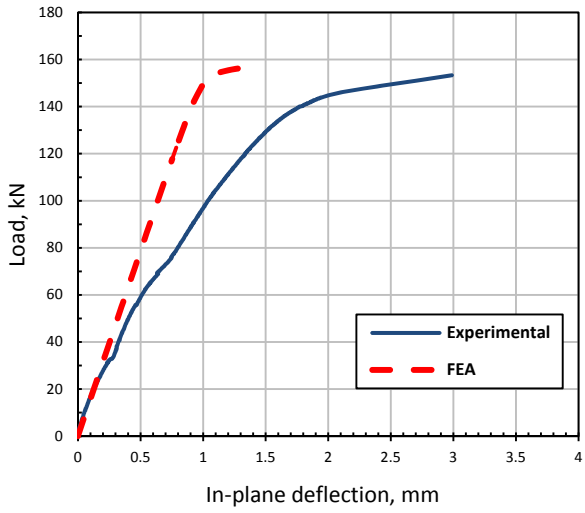

(**f**): CFRP specimen-SP-7.

Fig. (17): Verification curves of the simplified picture frame model.